Entanglement and bistability in coupled quantum dots inside a driven cavity

Arnab Mitra and Reeta Vyas
Department of Physics, University of Arkansas, Fayetteville, Arkansas 72701
(Received 1 April 2009; published 28 January 2010)

Generation and dissipation of entanglement between two coupled quantum dots (QDs) in a cavity driven by a coherent field is studied. We find that it is possible to generate and sustain a large amount of entanglement between the quantum dots in the steady state, even in the presence of strong decay in both the cavity and the dots. We investigate the effect of different parameters (decay rates, coupling strengths, and detunings) on entanglement. We find that the cavity field shows bistability and study the effect of relevant parameters on the existence of this bistable behavior. We also study the correlation between the cavity field and the entanglement between the dots. The experimental viability of the proposed scheme is discussed.

DOI: 10.1103/PhysRevA.81.012329 PACS number(s): 03.67.Bg, 78.67.Hc, 03.65.Ud, 42.55.Sa

I. INTRODUCTION

Several different schemes have been proposed for quantum computation and information processing devices. Most promising among them are schemes based on nuclear magnetic resonance (NMR) [1], trapped ions [2], cavity QED [3], Josephson junction [4], and solid-state-based [5–8] devices. Although these schemes have their own advantages and disadvantages, solid-state-based schemes continue to attract a lot of research interest both theoretically and experimentally. The reason is the tremendous progress that has been made in the past few years in achieving coherent control and manipulation of quantum dots (QDs)—tiny solid-state structures that can potentially act as qubits [9–17]. Now it is possible to experimentally create and manipulate such entangled qubits—the building block of quantum computers [9–12]. The fact that present-day computers are solid-state-based devices also plays an important role because engineering knowhow already exists for such devices.

All of the proposed *devices* face a daunting challenge in the form of decoherence. Although protocols like error correction codes [18] have been suggested to find ways to build fault-tolerant quantum computers, decoherence remains one of the main obstacles in the process of implementation of any quantum information or computation scheme. This is even more important for quantum-dot-based solid-state devices because quantum dots have a very short lifetime (typically of the order of 1–100 ps). Several new approaches to circumvent or at least minimize this problem have been suggested. These include heat bath-induced entanglement [19], reservoir engineering [20], quantum feedback control [21], and decay-enhanced entanglement [22].

We had previously studied a system of two quantum dots interacting with a coherent field inside a cavity and found that in the absence of any loss mechanism, it is possible to generate entanglement between the dots, although they can never be fully entangled [23]. In this work, we show that even in the presence of decay from both the quantum dots and the cavity, the dots could remain significantly entangled in the steady state. We also observe that the field inside the cavity shows bistability, which is not surprising because our system is similar in nature to a two-level atom inside a cavity, which is known to show bistability [24–27]. Possible correlation between the observed bistability and entanglement is a subject of huge interest. We also investigate this problem. The motivation is that if the field leaking outside the cavity enables us to calculate the entanglement, then it should be possible to manipulate it as well by changing the parameters of the system.

This article is organized as follows. Section II summarizes the model Hamiltonian of the system followed by a derivation of the Fokker-Planck equation for the dot and field variables. In Section III, we obtain the steady-state solution and investigate the optical bistability shown by the cavity field. Section IV describes the steady-state entanglement between the quantum dots and explores the correlation referred to earlier in terms of the cavity field statistics. We examine experimental feasibility for the range of parameters used in this article. Based on recent experiments on quantum dots [9–17], we conclude that these results are experimentally achievable. Section V summarizes the main results of this article.

II. HAMILTONIAN AND FOKKER-PLANCK EQUATION

We consider two identical quantum dots inside a cavity driven by a coherent field. The dots interact with the quantized field in the cavity via electric dipole interaction and are coupled to each other via the Forster interaction process [28]. There are two sources of decay—loss of cavity photons and the deexcitation of the dots. The Hamiltonian for the system that incorporate all these terms can be written as

$$\hat{H} = \omega_c \hat{a}^\dagger \hat{a} + \omega_d \hat{J}_z + ig(\hat{a}^\dagger \hat{J}_- - \hat{a}\hat{J}_+) + w(\hat{J}_{1+}\hat{J}_{2-} + \hat{J}_{1-}\hat{J}_{2+}) + i\varepsilon(\hat{a}^\dagger e^{-i\omega_0 t} - \hat{a}e^{i\omega_0 t}) + \hat{H}_{\text{Loss}}, \quad (1)$$

where we have chosen $\hbar = 1$, so that the Hamiltonian has the dimension of frequency. $\hat{a}(\hat{a}^\dagger)$ is the annihilation(creation) operator for the cavity photons characterized by resonance frequency ω_c; $\hat{J}_z$ is the dot excitation number operator, ω_d is the excitation energy of each dot, g is the coupling parameter for the dots and the cavity field interaction (taken to be identical for both dots), w represents the dot-dot interaction strength, and ε is the parameter coupling the cavity photons and the driving field of frequency ω_0 and provides a measure of the driving field amplitude. H_{Loss} describes dot and cavity field

losses. We can write the dot operators more explicitly as

$$\hat{J}_+ = \frac{1}{\sqrt{2}}\sum_{n=1}^{2}\hat{e}_n^\dagger\hat{h}_n^\dagger = \frac{1}{\sqrt{2}}(\hat{J}_{1+}+\hat{J}_{2+}),$$
$$\hat{J}_- = \frac{1}{\sqrt{2}}\sum_{n=1}^{2}\hat{e}_n\hat{h}_n = \frac{1}{\sqrt{2}}(\hat{J}_{1-}+\hat{J}_{2-}), \quad (2)$$
$$\hat{J}_z = \frac{1}{2}\sum_{n=1}^{2}(\hat{e}_n^\dagger\hat{e}_n+\hat{h}_n^\dagger\hat{h}_n)-\hat{I} = \hat{J}_{1z}+\hat{J}_{2z}-\hat{I}.$$

The basis states for the dots are the ground state $|J=1,M=-1\rangle \equiv |0\rangle \equiv |0\rangle_1 \bigotimes |0\rangle_2$, symmetric single-excitation state $|J=1,M=0\rangle \equiv |1\rangle \equiv \frac{1}{\sqrt{2}}[|0\rangle_1 \bigotimes |1\rangle_2 + |1\rangle_1 \bigotimes |0\rangle_2]$, biexcitation state $|J=1,M=1\rangle \equiv |2\rangle \equiv |1\rangle_1 \bigotimes |1\rangle_2$, and antisymmetric single exciton state $|J=0,M=0\rangle \equiv |1\rangle' \equiv \frac{1}{\sqrt{2}}[|0\rangle_1 \bigotimes |1\rangle_2 - |1\rangle_1 \bigotimes |0\rangle_2]$.

The basis states are the eigenstates of the excitation number operator $\hat{J}_z$. For mathematical convenience, we have defined $\hat{J}_z$ in such a way that the eigenvalues are symmetric with $\hat{J}_z|0\rangle = -|0\rangle$, $\hat{J}_z|1\rangle = 0$, $\hat{J}_z|2\rangle = |2\rangle$, and $\hat{J}_z|1\rangle' = 0$.

The dot-dot interaction $(\hat{J}_{1+}\hat{J}_{2-}+\hat{J}_{1-}\hat{J}_{2+})$ is also redefined as

$$\hat{T} = \hat{J}_{1+}\hat{J}_{2-}+\hat{J}_{1-}\hat{J}_{2+}+\hat{I}. \quad (3)$$

The eigenvectors and eigenvalues are given by $\hat{T}|0\rangle = |0\rangle$, $\hat{T}|1\rangle = 2|1\rangle$, $\hat{T}|2\rangle = |2\rangle$, and $\hat{T}|1\rangle' = 0$.

We have already seen that $\hat{J}_z|1\rangle' = 0$ and $\hat{T}|1\rangle' = 0$. One can easily check that $\hat{J}_+|1\rangle' = 0$ and $\hat{J}_-|1\rangle' = 0$ as well. Hence, the Hamiltonian has no effect on the antisymmetric state. $|1\rangle'$ is what is known as the optically inactive state; it does not interact with the other states. Physically it means that a system initially prepared in state $|1\rangle'$ will remain in the same state (or just pick up a phase) under the system Hamiltonian. Hence, while calculating the time evolution of the system, we can leave this state out and deal only with the other three.

In the $|0\rangle$, $|1\rangle$, $|2\rangle$ basis, the operators look like

$$\hat{J}_z = \begin{pmatrix}-1&0&0\\0&0&0\\0&0&1\end{pmatrix}, \quad \hat{J}_+ = \begin{pmatrix}0&0&0\\1&0&0\\0&1&0\end{pmatrix},$$
$$\hat{J}_- = \begin{pmatrix}0&1&0\\0&0&1\\0&0&0\end{pmatrix}, \quad \hat{T} = \begin{pmatrix}1&0&0\\0&2&0\\0&0&1\end{pmatrix}. \quad (4)$$

We can then rewrite the Hamiltonian in Eq. (1) in the following form:

$$\hat{H} = \hat{H}_0+\hat{H}_1,$$
$$\hat{H}_0 = \omega_0\hat{a}^\dagger\hat{a}+\omega_0\hat{J}_z, \quad (5)$$
$$\hat{H}_1 = \Delta_c\hat{a}^\dagger\hat{a}+\Delta_d\hat{J}_z+ig(\hat{a}^\dagger\hat{J}_- - \hat{a}\hat{J}_+) + i\varepsilon(\hat{a}^\dagger e^{-i\omega_0 t}-\hat{a}e^{i\omega_0 t})+w\hat{T}+\hat{H}_{\rm Loss},$$

where $\Delta_c = \omega_c-\omega_0$ and $\Delta_d = \omega_d-\omega_0$. We choose to work in the interaction picture by introducing the density matrix

$$\tilde{\rho} = e^{i\hat{H}_0 t}\rho e^{-i\hat{H}_0 t}. \quad (6)$$

The corresponding Hamiltonian is then

$$\tilde{\hat{H}}_1 = e^{i\hat{H}_0 t}\hat{H}_1 e^{-i\hat{H}_0 t} = \Delta_c\hat{a}^\dagger\hat{a}+\Delta_d\hat{J}_z+ig(\hat{a}^\dagger\hat{J}_- - \hat{a}\hat{J}_+) + i\varepsilon(\hat{a}^\dagger-\hat{a})+w\hat{T}+\tilde{\hat{H}}_{\rm Loss}. \quad (7)$$

We can write the equation of motion for the system density matrix following standard techniques [29,30]. For notational convenience, in what follows we write ρ for $\tilde{\rho}$. Then the master equation for the complete system can be written as

$$\dot{\rho} = -i\Delta_c[\hat{a}^\dagger\hat{a},\rho]-i\Delta_d[\hat{J}_z,\rho]+g[\hat{a}^\dagger\hat{J}_- - \hat{a}\hat{J}_+,\rho] + \varepsilon[\hat{a}^\dagger-\hat{a},\rho]-iw[\hat{T},\rho]+\frac{\gamma}{2}[2\hat{J}_-\rho\hat{J}_+ - \hat{J}_+\hat{J}_-\rho - \rho\hat{J}_+\hat{J}_-]+\kappa[2\hat{a}\rho\hat{a}^\dagger - \hat{a}^\dagger\hat{a}\rho-\rho\hat{a}^\dagger\hat{a}]. \quad (8)$$

Here we have introduced phenomenological constants γ and κ for the dot and cavity decay, respectively, using the standard procedure.

The usual method (see, for example, Refs. [29–32]) of mapping the operator master equation into a corresponding c-number equation using a normally ordered or symmetrically ordered characteristic function leads to differential equations containing derivatives of all orders that can then be truncated at the second order using system size expansion, provided the system contains a large number (N) of particles interacting with the field ($N \gg 1$). However, because our system consists of only two quantum dots, we cannot use this approach. Therefore, to derive a Fokker-Planck equation from Eq. (8), we follow the procedure employed in Refs. [33–36].

Let $|\alpha\rangle\langle\alpha|$ be the coherent state projector for the field and $\hat{\Lambda}$ act as the generic density operator for the QDs. In the triplet basis, $\hat{\Lambda}$ can be written as

$$\hat{\Lambda} = \begin{pmatrix}\frac{1}{3}+x & p & q\\ p^* & \frac{1}{3}-x-y & r\\ q^* & r^* & \frac{1}{3}+y\end{pmatrix}. \quad (9)$$

Here $\hat{\Lambda} = \sum_{i,j=0}^{2}\Lambda_{i,j}|i\rangle\langle j|$, where $|i\rangle$ and $|j\rangle$ could be $|0\rangle$, $|1\rangle$, or $|2\rangle$. As in any density matrix, the diagonal elements $\Lambda_{i,i}$ act as the population density for state $|i\rangle$ and the off-diagonal elements $\Lambda_{i,j}(i\neq j)$ measure the coherence between states $|i\rangle$ and $|j\rangle$. Thus, $\Lambda_{0,0} = (1/3+x)$ is the probability of finding the dots in the zero-exciton state $|0\rangle$. Similarly, $(1/3-x-y)$, and $(1/3+y)$ correspond to probabilities of finding the dots in states $|1\rangle$ and $|2\rangle$, respectively. The diagonal elements have been chosen in such a way as to guarantee that $\mathrm{Tr}(\hat{\Lambda}) = 1$. Off-diagonal element $\Lambda_{0,1} = p$ is the coherence between the ground state and the single-exciton state, $\Lambda_{0,2} = q$ is the coherence between the ground state and the biexciton state, and $\Lambda_{1,2} = r$ is the coherence between the single-exciton and the biexciton state. p^*, q^*, and r^* are simply the complex conjugates of p, q, and r.

By using $|\alpha\rangle\langle\alpha|$ as a basis for the field, and $\hat{\Lambda}$ as a basis for the dots, we can expand the complete system density operator ρ in the following form:

$$\hat{\rho} = \int P(\alpha,\alpha^*,x,y,p,p^*,q,q^*,r,r^*)\,|\alpha\rangle\langle\alpha| \times \hat{\Lambda}(x,y,p,p^*,q,q^*,r,r^*)\,d^2\alpha\,dx\,dy\,d^2p\,d^2q\,d^2r, \quad (10)$$

Together, $|\alpha\rangle\langle\alpha|\hat{\Lambda}$ acts as a projector for the complete system including both the field and the dots; and $P(\alpha, \alpha^*, x, y, p, p^*, q, q^*, r, r^*)$ behaves as a quasiprobability distribution for the field being in the state $|\alpha\rangle\langle\alpha|$ and the dots being in $\hat{\Lambda}(x, y, p, p^*, q, q^*, r, r^*)$, for given values of $\alpha, \alpha^* x, y, p, p^*, q, q^*, r$, and r^*.

In order to get a c-number equation from the operator master equation, we express the operators in Eq. (8) in terms of the projector $|\alpha\rangle\langle\alpha|\hat{\Lambda}$ and its derivatives as shown in Appendix. After doing so, we obtain the Fokker-Planck equation

$$\frac{\partial P}{\partial t} = \mathcal{L}\, P, \tag{11}$$

where

$$\begin{aligned}
\mathcal{L} = &-\frac{\partial}{\partial\alpha}[\varepsilon - (\kappa + i\Delta_c)\alpha + g(p^* + r^*)] - \frac{\partial}{\partial\alpha^*}[\varepsilon - (\kappa - i\Delta_c)\alpha^* + g(p + r)] + \frac{\partial}{\partial x}\left[\gamma\left(x + y - \frac{1}{3}\right) - g\alpha p - g\alpha^* p^*\right] \\
&+ \frac{\partial}{\partial y}\left[\gamma\left(y + \frac{1}{3}\right) + g\alpha r + g\alpha^* r^*\right] + \frac{\partial}{\partial p}\left[\gamma\left(\frac{p}{2} - r\right) + g\alpha^*(2x + y) - g\alpha q - i(w + \Delta_d)p\right] \\
&+ \frac{\partial}{\partial p^*}\left[\gamma\left(\frac{p^*}{2} - r^*\right) + g\alpha(2x + y) - g\alpha^* q^* + i(w + \Delta_d)p^*\right] + \frac{\partial}{\partial q}\left[\gamma\frac{q}{2} + g\alpha^*(p - r) - 2i\Delta_d q\right] \\
&+ \frac{\partial}{\partial q^*}\left[\gamma\frac{q^*}{2} + g\alpha(p^* - r^*) + 2i\Delta_d q^*\right] + \frac{\partial}{\partial r}[\gamma r - g\alpha^*(x + 2y) + g\alpha q + i(w - \Delta_d)r] \\
&+ \frac{\partial}{\partial r^*}[\gamma r^* - g\alpha(x + 2y) + g\alpha^* q^* - i(w - \Delta_d)r^*] - \frac{\partial^2}{\partial\alpha\partial x}g\left[x(p^* + r^*) - \frac{2p^* - r^*}{3}\right] \\
&- \frac{\partial^2}{\partial\alpha\partial y}g\left[y(p^* + r^*) + \frac{p^* + r^*}{3}\right] - \frac{\partial^2}{\partial\alpha\partial p}g\left[p(p^* + r^*) + \left(x + y - \frac{1}{3}\right)\right] - \frac{\partial^2}{\partial\alpha\partial p^*}g[p^*(p^* + r^*) - q^*] \\
&- \frac{\partial^2}{\partial\alpha\partial q}g[q(p^* + r^*) - r] - \frac{\partial^2}{\partial\alpha\partial q^*}g[q^*(p^* + r^*)] - \frac{\partial^2}{\partial\alpha\partial r}g\left[r(p^* + r^*) - \left(y + \frac{1}{3}\right)\right] - \frac{\partial^2}{\partial\alpha\partial r^*}g[r^*(p^* + r^*)] \\
&- \frac{\partial^2}{\partial\alpha^*\partial x}g\left[x(p + r) - \frac{2p - r}{3}\right] - \frac{\partial^2}{\partial\alpha^*\partial y}g\left[y(p + r) + \frac{p + r}{3}\right] - \frac{\partial^2}{\partial\alpha^*\partial p}g[p(p + r) - q] \\
&- \frac{\partial^2}{\partial\alpha^*\partial p^*}g\left[p^*(p + r) + \left(x + y - \frac{1}{3}\right)\right] - \frac{\partial^2}{\partial\alpha^*\partial q}g[q(p + r)] - \frac{\partial^2}{\partial\alpha^*\partial q^*}g[q^*(p + r) - r] \\
&- \frac{\partial^2}{\partial\alpha^*\partial r}g[r(p + r)] - \frac{\partial^2}{\partial\alpha^*\partial r^*}g\left[r^*(p + r) - \left(y + \frac{1}{3}\right)\right].
\end{aligned} \tag{12}$$

This equation has been obtained without the approximation of system size expansion and truncation of higher derivatives. By using the first-order derivatives or the drift terms of the Fokker-Planck equation, we can write the set of equations which determine the evolution of the mean value of the variables. The second-order derivatives lead to the diffusion matrix, which can be studied to investigate the noise and correlation among the variables. By using the drift terms, we obtain the mean value equation,

$$\begin{aligned}
\langle\dot{\alpha}\rangle &= \varepsilon - (\kappa + i\Delta_c)\langle\alpha\rangle + g(\langle p^*\rangle + \langle r^*\rangle), \\
\langle\dot{x}\rangle &= -\gamma\left(\langle x\rangle + \langle y\rangle - \frac{1}{3}\right) + g\langle\alpha p\rangle + g\langle\alpha^* p^*\rangle, \\
\langle\dot{y}\rangle &= -\gamma\left(\langle y\rangle + \frac{1}{3}\right) - g\langle\alpha r\rangle - g\langle\alpha^* r^*\rangle, \\
\langle\dot{p}\rangle &= -\gamma\left(\frac{\langle p\rangle}{2} - \langle r\rangle\right) - g(2\langle\alpha^* x\rangle + \langle\alpha^* y\rangle) \\
&\quad + g\langle\alpha q\rangle + i(w + \Delta_d)\langle p\rangle, \\
\langle\dot{q}\rangle &= -\gamma\frac{\langle q\rangle}{2} - g(\langle\alpha^* p\rangle - \langle\alpha^* r\rangle) + 2i\Delta_d\langle q\rangle,
\end{aligned}$$

$$\begin{aligned}
\langle\dot{r}\rangle = &-\gamma\langle r\rangle + g(\langle\alpha^* x\rangle + 2\langle\alpha^* y\rangle) - g\langle\alpha q\rangle \\
&- i(w - \Delta_d)\langle r\rangle.
\end{aligned} \tag{13}$$

Corresponding equations for $\langle\dot{\alpha^*}\rangle$, $\langle\dot{p^*}\rangle$, $\langle\dot{q^*}\rangle$, and $\langle\dot{r^*}\rangle$ can be obtained by taking the complex conjugate of Eq. (13). These equations are not closed as the mean values are coupled to second-order correlations, which in turn are coupled to even higher order correlations. Thus, we have an infinite hierarchy of coupled equations that, in general, cannot be solved. However, by writing the second-order average, say, $\langle x\, p\rangle$ as $\langle x\rangle\langle p\rangle + \langle\delta x\delta p\rangle$, where $\delta x = x - \langle x\rangle$ and $\delta p = p - \langle p\rangle$ represent noise in x and p, respectively, we see that if the noise terms are small compared with the mean values (low noise), we can use the approximation $\langle x\, p\rangle \approx \langle x\rangle\langle p\rangle$ in the equations for the means values. This is a valid approximation when the correlation between the dots and field are small in the lowest order. Previous works in similar systems have shown this to be the case (see, for example, Ref. [27]). With this approximation for the product terms in Eq. (13), we obtain a closed set of equations for the mean values. This approximation (referred to as factorization approximation) has been used extensively for a system of atoms in a cavity [29–33], and detailed numerical

solution of the corresponding Fokker-Planck equation shows that this approximation is justified when noise terms are small and gives fairly accurate results except near the turning points where the field inside the cavity can make a discontinuous jump (see, for example, Refs. [26,27]). It should be kept in mind that this approximation neglects noise correlation only in comparison to the mean values away from the turning points. To calculate noise correlations, one can use Eq. (12) to derive the equations for second-order correlations, and to solve them, one can make similar factorization approximations to decouple them from even higher order correlations. For our work, only the mean values of QD and field parameters are needed and diffusion terms [second-order differentials in Eq. (12)] do not affect mean values in this approximation.

III. STEADY-STATE SOLUTION AND BISTABILITY

In the steady state, the time derivatives are equal to zero. Although it is very cumbersome to write the analytical solutions for each variable, we can express the dot variables in terms of the field variable α and α^*. By doing so, we get

$$x = \frac{2\left(1+\delta_d^2\right)\left(1+W^2+\frac{\alpha\alpha^*}{4n_s}+\delta_d W+\frac{\delta_d^2}{4}\right)}{3K(\alpha,\alpha^*)},$$

$$y = -\frac{\left(1+\delta_d^2\right)\left(1+W^2+\frac{\alpha\alpha^*}{n_s}+\delta_d W+\frac{\delta_d^2}{4}\right)}{3K(\alpha,\alpha^*)},$$

$$p = -\frac{\alpha^*(1+i\delta_d)\left(1+iW+\frac{\alpha\alpha_*}{2n_s}-\frac{i\delta_d}{2}+\delta_d W+\frac{\delta_d^2}{2}\right)}{\sqrt{2n_s}K(\alpha,\alpha^*)},$$

$$q = \frac{\alpha^{*2}(1+i\delta_d)\left(1+iW+\frac{i\delta_d}{2}\right)}{2n_s K(\alpha,\alpha^*)},$$

$$r = -\frac{\alpha\alpha^{*2}(1+i\delta_d)}{(2n_s)^{3/2}K(\alpha,\alpha^*)}, \tag{14}$$

where

$$K(\alpha,\alpha^*) = \frac{3}{4}\frac{\alpha^2\alpha^{*2}}{n_s^2}+\left[\frac{\alpha\alpha^*}{n_s}+1+\left(W+\frac{\delta_d}{2}\right)^2\right]\left(1+\delta_d^2\right). \tag{15}$$

Equations for p^*, q^*, and r^* can be obtained by taking the complex conjugate of the corresponding equations for p, q, and r. Here we have defined saturation photon number n_s, scaled dot-dot interaction W, scaled dot detuning δ_d, cooperativity parameter C, and scaled cavity detuning δ_c, by

$$n_s = \frac{\gamma^2}{8g^2}, \quad W = \frac{2w}{\gamma}, \quad \delta_d = \frac{4\Delta_d}{\gamma}, \quad C = \frac{g^2}{\gamma\kappa}, \quad \delta_c = \frac{\Delta_c}{\kappa}. \tag{16}$$

By substituting expressions given in Eq. (14) into Eq. (13), and letting $\dot{\alpha}=0$ and $\dot{\alpha^*}=0$, we obtain

$$\alpha\left[(1+i\delta_c)+\frac{2C(1-i\delta_d)\left(1-iW+\frac{\alpha\alpha^*}{n_s}+\frac{i\delta_d}{2}+\delta_d W+\frac{\delta_d^2}{2}\right)}{K(\alpha,\alpha^*)}\right]-\frac{\varepsilon}{\kappa}=0,$$

$$\alpha^*\left[(1-i\delta_c)+\frac{2C(1+i\delta_d)\left(1+iW+\frac{\alpha\alpha^*}{n_s}-\frac{i\delta_d}{2}+\delta_d W+\frac{\delta_d^2}{2}\right)}{K(\alpha,\alpha^*)}\right]-\frac{\varepsilon}{\kappa}=0. \tag{17}$$

Introducing dimensionless driving field intensity Y^2 and intracavity field intensity X^2 as

$$X^2 = \frac{\alpha\alpha^*}{n_s}, \quad Y^2 = \frac{\varepsilon^2}{n_s\kappa^2}, \tag{18}$$

we can express a deterministic steady-state solution given by Eq. (17) as

$$Y^2 = X^2\left[\left(1+\frac{2C\left(1+X^2+\delta_d^2\right)}{K(X)}\right)^2+\left(\delta_c-\frac{2C\left[\delta_d X^2+\left(W+\frac{\delta_d}{2}\right)\left(1+\delta_d^2\right)\right]}{K(X)}\right)^2\right], \tag{19}$$

where

$$K(X) = \frac{3}{4}X^4+\left[X^2+1+\left(W+\frac{\delta_d}{2}\right)^2\right]\left(1+\delta_d^2\right). \tag{20}$$

Equation (19) indicates that the scaled intracavity intensity ($X^2=\alpha\alpha^*/n_s$) may show bistability as a function of the scaled driving field intensity [$Y^2=\varepsilon^2/(n_s\kappa^2)$], if $C\neq 0$. Thus, for optical bistability, cavity field-dot interaction must be present. Figures 1(a)–1(d) show plots of the scaled cavity field intensity X^2 as a function of the driving field intensity Y^2 for different values of parameters C, W, δ_d, and δ_c, respectively. For W and δ_d, the bistablity graphs converge at higher Y^2, meaning the cavity photon number does not depend on these parameters at strong pumping. However, they do not converge as C and δ_c are varied, in fact they diverge with changing δ_c at large field intensity. The reason behind this can be seen from Eqs. (19) and (20). When X is large, the inequalities $X^4 \gg X^2 \gg 1$ will hold. Hence, $K(X)$ can be approximated by just $3X^4/4$, which means Y^2 behaves as

$$Y^2 \sim X^2\left[\left(1+\frac{8C}{3X^2}\right)^2+\left(\delta_c-\frac{8C\delta_d}{3X^2}\right)^2\right]. \tag{21}$$

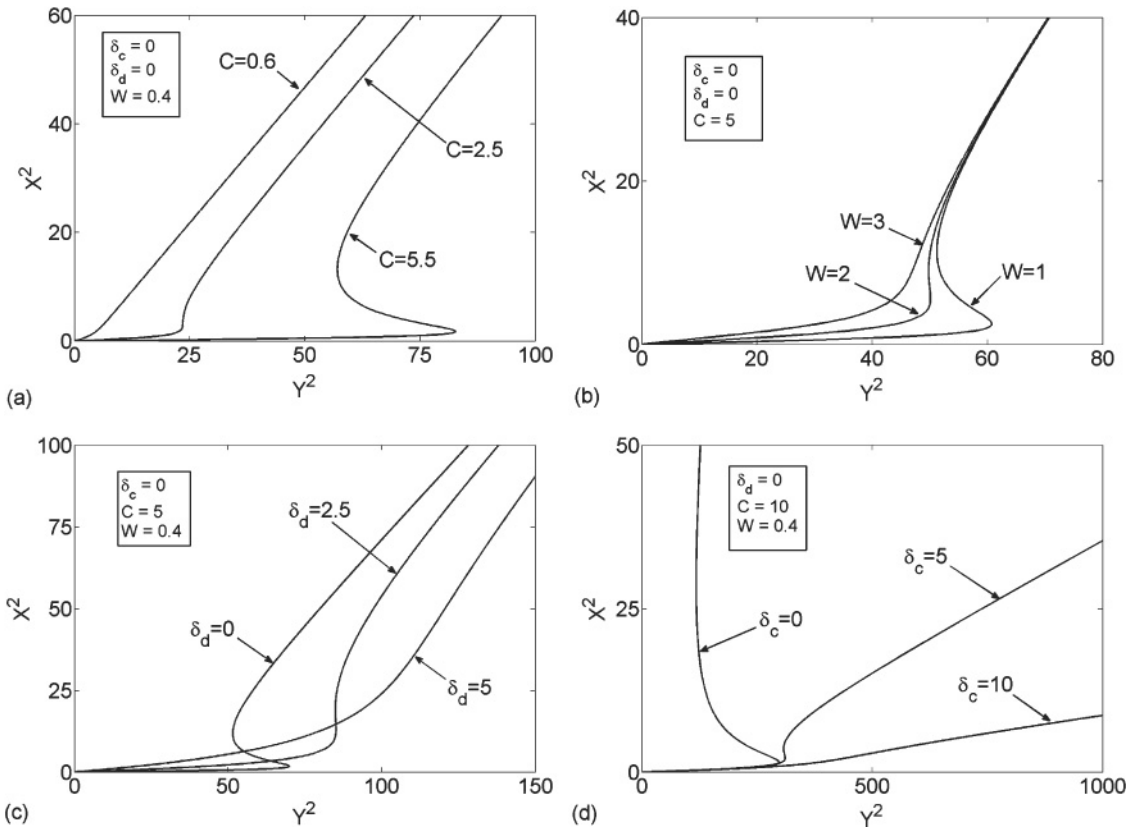

FIG. 1. Scaled cavity field intensity X^2 as a function of the scaled pump parameter Y^2 $[=\varepsilon^2/(n_s\kappa^2)]$ for different values of (a) cooperativity parameter C, (b) scaled dot-dot interaction parameter $W = 2w/\gamma$, (c) scaled dot detuning $\delta_d = 4\Delta_d/\gamma$, and (d) scaled cavity detuning $\delta_c = \Delta_c/\kappa$.

By neglecting terms proportional to $1/X^2$ and rearranging the terms, we can write

$$X^2 \approx \frac{1}{1+\delta_c^2}\left[Y^2 - \frac{16C}{3}(1-\delta_c\delta_d)\right]. \tag{22}$$

We can see, at large X, the $X^2 - Y^2$ curves should approach to straight lines with a slope $(1+\delta_c^2)^{-1}$ and intercept $[(-16C/3)(1-\delta_c\delta_d)/(1+\delta_c^2)]$. This explains why they should converge with varying W and δ_d, as X becomes independent of W and of δ_d (if $\delta_c = 0$). This trend is clearly seen in Fig. 1(b). Figure 1(c) shows convergence of the bistability plots at much larger values of X. With increasing δ_c, the slope decreases and the lines diverge as in Fig. 1(d). Changing C simply changes the intercepts that makes the lines parallel (Fig. 1(a)). Physically, this linearity means that at sufficiently strong pumping, the effect of dots on the cavity field become negligible and the cavity field intensity becomes simply proportional to the driving field intensity.

IV. ENTANGLEMENT BETWEEN THE DOTS

To calculate entanglement between the two quantum dots, we obtain numerical solutions of Eq. (13), which give the values of α and α^* in the steady state. Out of many solutions, the correct ones are chosen on the physical ground that mean values of α and α^* (without the noise terms) must be complex conjugate of each other. By plugging back the values of α and α^* in Eq. (14), we get the matrix elements for the QDs. Matrix Λ of Eq. (9) is expressed in terms of the basis vectors $|00\rangle$, $\frac{1}{\sqrt{2}}(|01\rangle + |10\rangle)$, and $|11\rangle$. When we reexpress Λ in the basis $|00\rangle$, $|01\rangle$, $|10\rangle$, and $|11\rangle$, the complete 4×4 density matrix of the two quantum dots takes the form

$$\rho = \begin{pmatrix} \frac{1}{3}+x & \frac{p}{\sqrt{2}} & \frac{p}{\sqrt{2}} & q \\ \frac{p^*}{\sqrt{2}} & \frac{\frac{1}{3}-x-y}{2} & \frac{\frac{1}{3}-x-y}{2} & \frac{r}{\sqrt{2}} \\ \frac{p^*}{\sqrt{2}} & \frac{\frac{1}{3}-x-y}{2} & \frac{\frac{1}{3}-x-y}{2} & \frac{r}{\sqrt{2}} \\ q^* & \frac{r^*}{\sqrt{2}} & \frac{r^*}{\sqrt{2}} & \frac{1}{3}+y \end{pmatrix}. \tag{23}$$

Once we have the complete density matrix of the two-dot system, we can then calculate the concurrence as a measure of the entanglement between the two dots in the steady state. To calculate concurrence, we obtain the matrix $\tilde{\rho} = (\sigma_y \bigotimes \sigma_y)\rho^*(\sigma_y \bigotimes \sigma_y)$, where σ_y is the Pauli spin matrix $\left(\begin{smallmatrix} 0 & -i \\ i & 0 \end{smallmatrix}\right)$ and ρ^* is complex conjugate of ρ. If λ_1, λ_2, λ_3, and λ_4 are the square roots of the eigenvalues of the matrix $\rho\tilde{\rho}$ in descending order, then concurrence of the system is defined as [37]

$$C(\rho) = \max[0, \lambda_1 - \lambda_2 - \lambda_3 - \lambda_4], \tag{24}$$

where $\max[0, x]$ is the larger number between 0 and x.

In Figs. 2(a)–2(f), we have plotted the steady-state entanglement (concurrence) as a function of the driving field strength ε along the x axis and one other parameter (κ, γ, W, δ_c, δ_d,

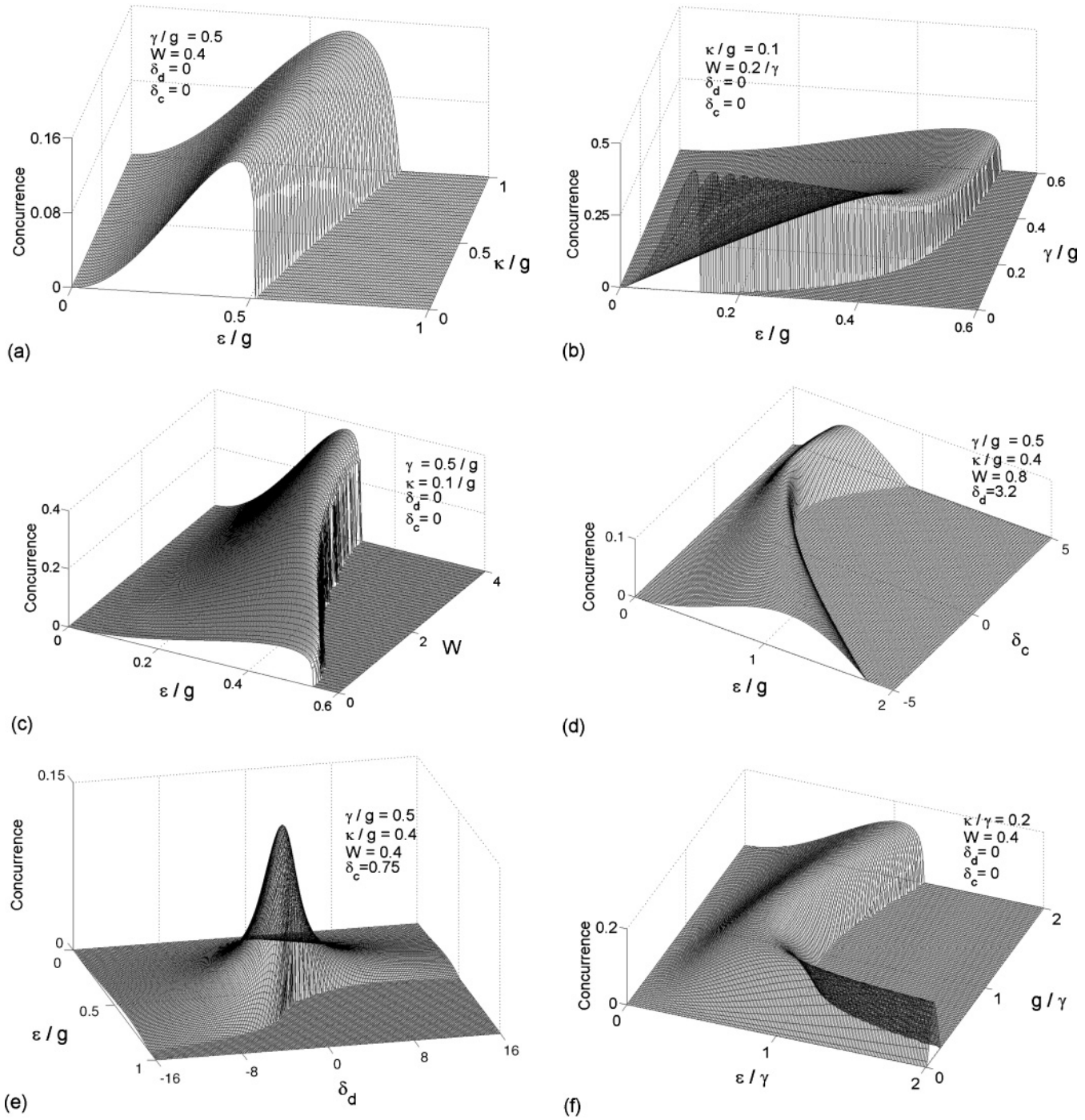

FIG. 2. Concurrence as a function of pump parameter ε (in units of g for figures a–e and in units of γ in figure f) along the x axis and one other parameter along the y axis. The y axis represents (a) dimensionless cavity decay rate κ/g, (b) dimensionless dot decay rate γ/g, (c) scaled dot-dot interaction parameter $W = 2w/\gamma$, (d) scaled cavity detuning $\delta_c = \Delta_c/\kappa$, (e) scaled dot detuning $\delta_d = 4\Delta_d/\gamma$, and (f) scaled dot-field coupling g/γ.

and g, respectively) along the y axis. In all of these graphs, the concurrence builds up with increasing driving field up to a maximum value and then rapidly falls to zero. It stays at zero with a further increase in driving field.

This phenomenon can be explained as follows: Starting from an unentangled state (ground state), the two QDs become more entangled with an increase in the cavity field intensity, as the cavity field helps in coherent mixing among the zero-exciton, single-exciton, and biexciton states. However, as the driving field intensity increases further, the cavity field increases rapidly, resulting in the dots in an equal mixture of the three states (zero-, one-, and two-exciton states), with virtually no coherence between them. This leads the entanglement to fall sharply and eventually become zero. Further discussion of this is presented later in connection with correlation between concurrence and optical bistability.

Several interesting features can be observed from these graphs that tell us how the choice of dot and cavity parameters affect entanglement. In Fig. 2(a), concurrence is plotted against the scaled driving field strength ε/g and scaled cavity decay rate κ/g. We find that for larger κ, maximum concurrence is reached at larger value of ε. However, maximum possible steady-state concurrence between the dots remains almost the same for different values of κ. This means faster cavity decay only requires a stronger driving field to produce the same amount of entanglement.

This is in sharp contrast to Fig. 2(b), which shows the effect of dot decay rate γ. Maximum concurrence is highest at $\gamma = 0$ and decreases with increasing γ. Hence, the potential to create entanglement is maximum in the absence of any dot decay mechanism and the faster the dot decay rate, the lower the amount of entanglement that can be generated. Intuitively, this makes sense that cavity decay does not but dot decay does diminish the potential to create dot-dot entanglement. Also, we can see from Eq. (14), the dot parameters x, y, p, q, and r do not have explicit κ dependence, but they depend on the value of γ. Interestingly, though, the concurrence is not 1 even when $\gamma = 0$, and it is not always 0 at large values of γ; in fact it asymptotically attains a steady value. Hence, the dots cannot be fully entangled even in the absence of decay, but it is possible to create some entanglement even in the presence of very large decay. Figure 2(c) shows that concurrence increases with dot-dot coupling W. However, increasing W does not increase concurrence indefinitely but takes it to an asymptotic value.

Next we compare the effects of the two detuning parameters δ_c and δ_d on the concurrence. Figure 2(d) shows that with change in δ_c, the value of the pump parameter ε at which the maximum concurrence is achieved also changes. We also find that, similar to the cavity decay rate κ, the maximum concurrence the dots can achieve is insensitive to the cavity detuning δ_c. Moreover, the concurrence plot is not symmetric about $\delta_c = 0$ unless both W and δ_d are zero. This is expected because the presence of dot-dot coupling shifts the energy levels of the dots. Thus, for nonzero W and δ_d, the dots are no longer in resonance with ω_0 resulting in asymmetry in δ_c. This asymmetry is evident from Eq. (19), which shows that for nonzero W or δ_d, the field amplitudes are not the same for $\pm\delta_c$. The asymmetry in field amplitude makes concurrence also asymmetric in δ_c.

Things are very different with dot detuning δ_d as shown in Fig. 2(e). With increasing δ_d, maximum concurrence decreases rapidly, and at significant detuning, virtually no concurrence can be generated. Hence, it is important to have the dot excitation frequency close to resonance. But again, the concurrence plot is not always symmetric about $\delta_d = 0$ and maximum concurrence may not be achieved at exact resonance. From Eq. (19), the cavity field is an even function of δ_d only when $\delta_c = 0$ and $W = 0$ or $(-\delta_d/2)$.

In Fig. 2(f), we have plotted concurrence as a function of g (in units of γ) — which shows the effect of the coupling parameter between the dot and the quantized field on concurrence, for a fixed dot decay rate. As expected, concurrence remains zero at $g = 0$ because this represents no interaction between the dots and the field and, hence, no chance for the dots to ever go to the excited state. But, for a finite g, however small, concurrence exists. Not only that, the maximum possible concurrence that can be generated is the same at all values of $g > 0$ (all other parameters being equal). However, at very small values of g $(0 < g \ll 1)$, it takes a very strong driving field to reach that maximum concurrence (in the figure, we have not shown the gradual increase of the concurrence to the maximum value and the decrease to zero for small values of g). Another interesting feature that we can observe is, starting from zero, initially an increase in g lowers the driving field required to attain the maximum concurrence. However, this trend reverses for higher values of g where a stronger driving field is required to produce the maximum possible concurrence at larger g. Although apparently counterintuitive, this result is consistent with the observation in Ref. [23] that large dot-field interaction actually acts against formation of dot-dot entanglement.

Hence, we observe that to maximize concurrence, one should maximize the dot-dot interaction W and minimize the dot decay rate γ and the dot detuning δ_d. Dot-field interaction strength g, cavity decay rate κ, and cavity detuning δ_c do not change the value of the maximum possible concurrence, although they affect at what driving field strength that concurrence can be achieved. For the case of two coupled dots inside a cavity driven by a field, the maximum value of concurrence obtained in the limit $(w \gg g, \gamma \to 0, \Delta_d \to 0)$ is found to be 0.43.

Figure 3 shows steady-state concurrence and the scaled cavity field intensity $(X^2/50)$ as a function of the driving field ε for three values of g. We can see that, as the driving field is increased, the cavity field starts to build up and so does the concurrence. In the regime of bistability, the corresponding concurrence curve reaches its maximum near the edge of the lower branch of the bistability curve. With further increases in the driving field, concurrence decreases very rapidly and falls to zero just at the transition point of the bistability curve. With an even stronger driving field, as the cavity field tracks the upper branch of the bistability curve, concurrence stays at zero. However, if the field does not show bistability, the corresponding concurrence curve shows a much smoother behavior. Hence, a sharp rise and fall in concurrence is accompanied by the presence of strong bistability. This is a

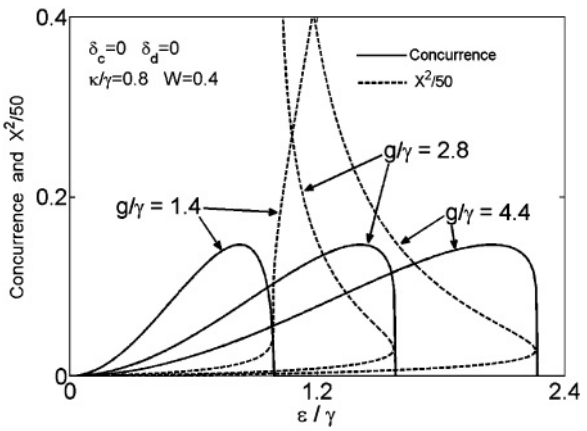

FIG. 3. Concurrence C and scaled cavity field intensity $X^2/50$ plotted against scaled pump parameter ε/γ for three different sets of values of scaled dot-field coupling g/γ.

remarkably interesting phenomenon that tells us if the cavity field shows bistability, then by measuring the field leaking outside the cavity, an observer should be able to determine the presence or absence of entanglement between the dots. By adjusting the driving field strength appropriately and hence controlling the field inside the cavity, one can switch the entanglement on and off. We find that with increasing photon density inside the cavity, the dots closely resemble the state

$$\hat{\Lambda} \approx \begin{pmatrix} \frac{1}{3} & 0 & 0 \\ 0 & \frac{1}{3} & 0 \\ 0 & 0 & \frac{1}{3} \end{pmatrix}; \tag{25}$$

that is, x, y, p, p^*, q, q^*, r, and r^* in Eq. (9) tend toward 0 (typical values of x, y, p... are of the order of 0.001). In other words, the state of the dots can accurately be described as an equal mixture of the zero-exciton, single-exciton, and biexciton states, each with probability $\frac{1}{3}$. Because our single-exciton state $|1\rangle = \frac{1}{\sqrt{2}}(|0\rangle_1 \bigotimes |1\rangle_2 + |1\rangle_1 \bigotimes |0\rangle_2)$ is itself an entangled state, it might appear that even in this final steady state there should be some entanglement left between the dots. However, when we express the complete density matrix in the usual $|00\rangle$, $|01\rangle$, $|10\rangle$ and $|11\rangle$ basis, we obtain

$$\rho = \begin{pmatrix} \frac{1}{3} & 0 & 0 & 0 \\ 0 & \frac{1}{6} & \frac{1}{6} & 0 \\ 0 & \frac{1}{6} & \frac{1}{6} & 0 \\ 0 & 0 & 0 & \frac{1}{3} \end{pmatrix}, \tag{26}$$

which has concurrence zero, meaning no entanglement. The reason is that this density matrix could be obtained as a statistical mixture of purely unentangled states.

Following Ref. [38], if in the Bell basis a density matrix can be written as

$$(p_1|\Phi^+\rangle\langle\Phi^+| + p_2|\Phi^-\rangle\langle\Phi^-| + p_3|\Psi^+\rangle\langle\Psi^+| + p_4|\Psi^-\rangle\langle\Psi^-|),$$

where

$$\begin{aligned} |\Phi^+\rangle &= \frac{1}{\sqrt{2}}[|00\rangle + |11\rangle], \\ |\Phi^-\rangle &= i\frac{1}{\sqrt{2}}[|00\rangle - |11\rangle], \\ |\Psi^+\rangle &= i\frac{1}{\sqrt{2}}[|01\rangle + |10\rangle], \\ |\Psi^-\rangle &= \frac{1}{\sqrt{2}}[|01\rangle - |10\rangle] \end{aligned} \tag{27}$$

are the modified Bell states, and none of p_1, p_2, p_3, and p_4 is greater than (1/2), then it is always possible to find phase constant θ_js such that

$$\sum_{j=1}^{4} p_j e^{i\theta_j} = 0 \tag{28}$$

and recreate the density matrix as an equal mixture of the following set of eight states:

$$\begin{aligned} &\sqrt{p_1}e^{i\theta_1/2}|\Phi^+\rangle \pm \sqrt{p_2}e^{i\theta_2/2}|\Phi^-\rangle \pm \sqrt{p_3}e^{i\theta_3/2}|\Psi^+\rangle \\ &\quad \pm \sqrt{p_4}e^{i\theta_4/2}|\Psi^-\rangle. \end{aligned}$$

Each of these states is an unentangled state, implying that the overall state will also be unentangled.

In our case, $p_1 = 1/3$, $p_2 = 1/3$, $p_3 = 1/3$, and $p_4 = 0$. If we choose θ_j's so that Eq. (28) is satisfied (e.g., $\theta_1 = \pi/3, \theta_2 = -\pi/3$ and $\theta_3 = \pi$), we get the following four unentangled states:

$$\begin{aligned} &\frac{1}{\sqrt{6}}[(e^{i\pi/6} + ie^{-i\pi/6})|0\rangle_1 + |1\rangle_1] \\ &\qquad \bigotimes [|0\rangle_2 + (e^{i\pi/6} - ie^{-i\pi/6})|1\rangle_2], \\ &\frac{1}{\sqrt{6}}[(e^{i\pi/6} + ie^{-i\pi/6})|0\rangle_1 - |1\rangle_1] \\ &\qquad \bigotimes [|0\rangle_2 - (e^{i\pi/6} - ie^{-i\pi/6})|1\rangle_2], \\ &\frac{1}{\sqrt{6}}[(e^{i\pi/6} - ie^{-i\pi/6})|0\rangle_1 + |1\rangle_1] \\ &\qquad \bigotimes [|0\rangle_2 + (e^{i\pi/6} + ie^{-i\pi/6})|1\rangle_2], \\ &\frac{1}{\sqrt{6}}[(e^{i\pi/6} - ie^{-i\pi/6})|0\rangle_1 - |1\rangle_1] \\ &\qquad \bigotimes [|0\rangle_2 - (e^{i\pi/6} + ie^{-i\pi/6})|1\rangle_2]. \end{aligned}$$

These states can reproduce the density matrix given in Eq. (26) when mixed in equal (one-fourth) proportion. Any other choice of θ satisfying Eq. (27) would also reproduce ρ from an ensemble of unentangled states.

Next we examine whether the results described in the preceding discussion can be observed with current experimental techniques. Several recent experiments using GaAs quantum dots have shown that it is possible to optically manipulate the coherent evolution of one [10] or more [11] dot(s). Charge-entangled state preparation has been possible in one (or two) quantum dots using GaAs and InAs dots [9]. All optical quantum gate operations have also been carried out on a single GaAs quantum dot [12]. Here we show that the range of parameters needed to observe the features described in Figs. 1, 2, and 3 can be achieved experimentally. We have the following parameters associated with the complete dot-cavity-pump system: cavity-pump coupling ε, cavity-dot coupling g, dot-dot coupling w, dot decay rate γ, cavity decay rate κ, dot detuning Δ_d, and cavity detuning Δ_c. Of these, the two detuning parameters can be adjusted, and for simplicity, we choose to be zero. The energy band gap in typical GaAs quantum dots is about 1.6 eV, which requires an excitation wavelength in the vicinity of 900 nm for resonance. The experimentally observed value of g for GaAs dots is of the order of 0.1 meV [13]. Possible interdot coupling w due to the Forster interaction has been calculated by Lovett *et al.* [14] and Unold *et al.* [15]. They estimated that depending on the material, shape, size, and distance among the dots, w can be of the order of 0.01 meV to 1 meV. Experimentally observed dephasing time for GaAs dots [10] is ~40 ps, which gives $\gamma \sim 15$ μeV. However, quantum dots with ultra-long dephasing times have been experimentally observed, as in Ref. [16], where InGaAs dots with lifetime >600 ps have been observed, giving $\gamma \sim 1$ μeV. Modern optical cavities can have a very

long lifetime and a correspondingly small decay rate. It is not unusual to have an optical cavity lifetime in excess of 10 ns [17], giving $\kappa < 0.1$ μeV. Finally, the cavity-pump coupling ε, which depends on the strength of the driving field, can be adjusted as required.

As an example, scaled parameters in Fig. 2(a) are $\gamma/g = 0.5$, $W = 2w/\gamma = 0.4$, κ/g between 0 and 1, ε/g between 0 and 1, and $\Delta_d = \Delta_c = 0$. In terms of unscaled value of $g = 0.1$ meV, values of other parameters correspond to $\gamma = 0.05$ meV, $w = 0.01$ meV, κ between 0 and 0.1 meV, and ε between 0 and 0.1 meV, all within an existing range of experimentally achievable parameter values. The bistability curves shown in Fig. 1(a) can be observed using unscaled parameters $w = 0.01$ meV, $g = 0.1$ meV, $\gamma = 0.05$ meV, and $\kappa = 0.3$ to 0.04 meV. Similarly, we can show that the features in other graphs of Figs. 1, 2, and 3 can be experimentally realized.

V. CONCLUSION

We have studied the dynamics of two coupled quantum dots interacting with a cavity driven by a coherent field. We have observed that starting from an initially unentangled state, it is possible to generate and sustain significant entanglement between the dots in the steady state for nonzero cavity-dot coupling ($g \neq 0$), even in the presence of both dot decay and cavity decay. Maximum entanglement in steady state increases with an increase in dot-dot coupling and decreases with increased dot decay rate and dot detuning. The maximum entanglement the system can achieve is not significantly affected by the dot-field coupling strength, cavity decay rate, and cavity detuning, but maximum entanglement is achieved at a much larger value of the driving field. We also find that for large values of cavity-dot coupling, the cavity field shows bistable behavior and appears to be strongly correlated with the entanglement between the dots. With an increase in the driving field, both cavity field intensity and dot-dot entanglement increase. As the cavity field nears the edge of the lower branch of the bistability curve, entanglement starts to decrease rapidly and falls to zero at the transition point. No steady-state entanglement between the dots is found when the cavity field follows the upper branch of the bistability curve. Hence, by changing the external driving field, entanglement between the dots can be turned on and off. With recent advances in quantum dot technology, it is possible to observe these results experimentally.

ACKNOWLEDGMENTS

The authors wish to thank S. Singh for many helpful discussions.

APPENDIX

To obtain the Fokker-Planck equation, we convert the operator equation given in Eq. (8) into a c-number equation. We use properties for field operators given in Ref. [33] [see Eq. (18)] and the following properties for the dot operators:

$$\hat{J}_z\hat{\Lambda} = \begin{pmatrix} -\frac{1}{3}-x & -p & -q \\ 0 & 0 & 0 \\ q^* & r^* & \frac{1}{3}+y \end{pmatrix}$$
$$= \frac{1}{3}(y-x)\hat{I} - \frac{1}{3}(1+2x+y)\frac{\partial\hat{\Lambda}}{\partial x} + \frac{1}{3}(1+x+2y)\frac{\partial\hat{\Lambda}}{\partial y} - p\frac{\partial\hat{\Lambda}}{\partial p} - q\frac{\partial\hat{\Lambda}}{\partial q} + q^*\frac{\partial\hat{\Lambda}}{\partial q^*} + r^*\frac{\partial\hat{\Lambda}}{\partial r^*},$$
$$\hat{\Lambda}\hat{J}_z = \begin{pmatrix} -\frac{1}{3}-x & 0 & q \\ -p^* & 0 & r \\ -q^* & 0 & \frac{1}{3}+y \end{pmatrix}$$
$$= \frac{1}{3}(y-x)\hat{I} - \frac{1}{3}(1+2x+y)\frac{\partial\hat{\Lambda}}{\partial x} + \frac{1}{3}(1+x+2y)\frac{\partial\hat{\Lambda}}{\partial y} + q\frac{\partial\hat{\Lambda}}{\partial q} + r\frac{\partial\hat{\Lambda}}{\partial r} - p^*\frac{\partial\hat{\Lambda}}{\partial p^*} - q^*\frac{\partial\hat{\Lambda}}{\partial q^*}, \tag{A1}$$
$$\hat{J}_+\hat{\Lambda} = (\hat{\Lambda}\hat{J}_-)^\dagger = \begin{pmatrix} 0 & 0 & 0 \\ \frac{1}{3}+x & p & q \\ p^* & \frac{1}{3}-x-y & r \end{pmatrix}$$
$$= \frac{1}{3}(p+r)\hat{I} - \frac{1}{3}(p+r)\frac{\partial\hat{\Lambda}}{\partial x} + \frac{1}{3}(2r-p)\frac{\partial\hat{\Lambda}}{\partial y} + q\frac{\partial\hat{\Lambda}}{\partial r} + \left(\frac{1}{3}+x\right)\frac{\partial\hat{\Lambda}}{\partial p^*} + p^*\frac{\partial\hat{\Lambda}}{\partial q^*} + \left(\frac{1}{3}-x-y\right)\frac{\partial\hat{\Lambda}}{\partial r^*},$$
$$\hat{\Lambda}\hat{J}_+ = (\hat{J}_-\hat{\Lambda})^\dagger = \begin{pmatrix} p & q & 0 \\ \frac{1}{3}-x-y & r & 0 \\ r^* & \frac{1}{3}+y & 0 \end{pmatrix}$$
$$= \frac{1}{3}(p+r)\hat{I} + \frac{1}{3}(2p-r)\frac{\partial\hat{\Lambda}}{\partial x} - \frac{1}{3}(p+r)\frac{\partial\hat{\Lambda}}{\partial y} + q\frac{\partial\hat{\Lambda}}{\partial p} + \left(\frac{1}{3}-x-y\right)\frac{\partial\hat{\Lambda}}{\partial p^*} + r^*\frac{\partial\hat{\Lambda}}{\partial q^*} + \left(\frac{1}{3}+y\right)\frac{\partial\hat{\Lambda}}{\partial r^*}, \tag{A2}$$
$$\hat{T}\hat{\Lambda} = \begin{pmatrix} \frac{1}{3}+x & p & q \\ 2p^* & 2\left(\frac{1}{3}-x-y\right) & 2r \\ q^* & r^* & \frac{1}{3}+y \end{pmatrix}$$
$$= \frac{1}{3}(4-3x-3y)\hat{I} - \frac{1}{3}\left(\frac{1}{3}-4x-y\right)\frac{\partial\hat{\Lambda}}{\partial x} - \frac{1}{3}\left(\frac{1}{3}-x-4y\right)\frac{\partial\hat{\Lambda}}{\partial y} + p\frac{\partial\hat{\Lambda}}{\partial p} + q\frac{\partial\hat{\Lambda}}{\partial q} + 2r\frac{\partial\hat{\Lambda}}{\partial r}$$

$$+2p^*\frac{\partial\hat{\Lambda}}{\partial p^*}+q^*\frac{\partial\hat{\Lambda}}{\partial q^*}+r^*\frac{\partial\hat{\Lambda}}{\partial r^*},$$

$$\hat{\Lambda}\hat{T}=\begin{pmatrix}\frac{1}{3}+x & 2p & q\\ p^* & 2\left(\frac{1}{3}-x-y\right) & r\\ q^* & 2r^* & \frac{1}{3}+y\end{pmatrix}$$

$$=\frac{1}{3}(4-3x-3y)\hat{I}-\frac{1}{3}\left(\frac{1}{3}-4x-y\right)\frac{\partial\hat{\Lambda}}{\partial x}$$
$$-\frac{1}{3}\left(\frac{1}{3}-x-4y\right)\frac{\partial\hat{\Lambda}}{\partial y}+2p\frac{\partial\hat{\Lambda}}{\partial p}+q\frac{\partial\hat{\Lambda}}{\partial q}+r\frac{\partial\hat{\Lambda}}{\partial r}$$
$$+p^*\frac{\partial\hat{\Lambda}}{\partial p^*}+q^*\frac{\partial\hat{\Lambda}}{\partial q^*}+2r^*\frac{\partial\hat{\Lambda}}{\partial r^*}, \tag{A3}$$

$$2\hat{J}_-\hat{\Lambda}\hat{J}_+-\hat{J}_+\hat{J}_-\hat{\Lambda}-\hat{\Lambda}\hat{J}_+\hat{J}_-$$
$$=\begin{pmatrix}2\left(\frac{1}{3}-x-y\right) & -p+2r & -q\\ -p^* & 2(x+2y) & -2r\\ -q^* & -2r^* & -2\left(\frac{1}{3}+y\right)\end{pmatrix}$$
$$=2\left(\frac{1}{3}-x-y\right)\frac{\partial\hat{\Lambda}}{\partial x}-2\left(\frac{1}{3}+y\right)\frac{\partial\hat{\Lambda}}{\partial y}-(p-2r)\frac{\partial\hat{\Lambda}}{\partial p}$$
$$-q\frac{\partial\hat{\Lambda}}{\partial q}-2r\frac{\partial\hat{\Lambda}}{\partial r}-(p^*-2r^*)\frac{\partial\hat{\Lambda}}{\partial p^*}$$
$$-q^*\frac{\partial\hat{\Lambda}}{\partial q^*}-2r^*\frac{\partial\hat{\Lambda}}{\partial r^*}. \tag{A4}$$

Using these operator relations, we can convert Eq. (8) to a corresponding equation for $P(\alpha,\alpha^*,x,y,p,p^*,q,q^*,r,r^*)$. As an example, we consider the second term $[\hat{J}_z,\rho]$, which can be written as

$$(J_z\rho-\rho J_z)$$
$$=\int P\ |\alpha\rangle\langle\alpha|\ \left(J_z\hat{\Lambda}-\Lambda J_z\right)\ d^2\alpha\ dx\ dy\ d^2p\ d^2q\ d^2r$$
$$=\int P\ |\alpha\rangle\langle\alpha|\left[\left(-p\frac{\partial}{\partial p}+p^*\frac{\partial}{\partial p^*}-2q\frac{\partial}{\partial q}+2q^*\frac{\partial}{\partial q^*}\right.\right.$$
$$\left.\left.-\ r\frac{\partial}{\partial r}+r^*\frac{\partial}{\partial r^*}\right)\hat{\Lambda}\right]d^2\alpha\ dx\ dy\ d^2p\ d^2q\ d^2r$$
$$=\int|\alpha\rangle\langle\alpha|\,\hat{\Lambda}\left[\left(\frac{\partial}{\partial p}p-\frac{\partial}{\partial p^*}p^*+\frac{\partial}{\partial q}2q-\frac{\partial}{\partial q^*}2q^*\right.\right.$$
$$\left.\left.+\ \frac{\partial}{\partial r}r-\frac{\partial}{\partial r^*}r^*\right)\ P\right]d^2\alpha\ dx\ dy\ d^2p\ d^2q\ d^2r. \tag{A5}$$

In the last step, we have changed the derivative from $\hat{\Lambda}$ to P, using the rules of partial integration, which leaves a minus sign. This is valid as long as the quasiprobability function P vanishes at the boundary. After calculating each of the remaining terms in a similar fashion, we finally write the equation for P as

$$\int|\alpha\rangle\langle\alpha|\ \hat{\Lambda}\ \frac{\partial P}{\partial t}\ d^2\alpha\ dx\ dy\ d^2p\ d^2q\ d^2r$$
$$=\int|\alpha\rangle\langle\alpha|\ \hat{\Lambda}\left\{-\frac{\partial}{\partial\alpha}[\varepsilon-(\kappa+i\Delta_c)\alpha+g(p^*+r^*)]\right.$$
$$-\frac{\partial}{\partial\alpha^*}[\varepsilon-(\kappa-i\Delta_c)\alpha^*+g(p+r)]$$
$$+\frac{\partial}{\partial x}\left[\gamma\left(x+y-\frac{1}{3}\right)-g\alpha p-g\alpha^*p^*\right]$$
$$+\frac{\partial}{\partial y}\left[\gamma\left(y+\frac{1}{3}\right)+g\alpha r+g\alpha^*r^*\right]$$
$$+\frac{\partial}{\partial p}\left[\gamma\left(\frac{p}{2}-r\right)+g\alpha^*(2x+y)-g\alpha q\right.$$
$$\left.-\ i(w+\Delta_d)p\right]+\frac{\partial}{\partial p^*}\left[\gamma\left(\frac{p^*}{2}-r^*\right)+g\alpha(2x+y)\right.$$
$$\left.-\ g\alpha^*q^*+i(w+\Delta_d)p^*\right]$$
$$+\frac{\partial}{\partial q}\left[\gamma\frac{q}{2}+g\alpha^*(p-r)-2i\Delta_dq\right]$$
$$+\frac{\partial}{\partial q^*}\left[\gamma\frac{q^*}{2}+g\alpha(p^*-r^*)+2i\Delta_dq^*\right]$$
$$+\frac{\partial}{\partial r}[\gamma r-g\alpha^*(x+2y)+g\alpha q+i(w-\Delta_d)r]$$
$$+\frac{\partial}{\partial r^*}[\gamma r^*-g\alpha(x+2y)+g\alpha^*q^*-i(w-\Delta_d)r^*]$$
$$-\frac{\partial^2}{\partial\alpha\partial x}g\left[x(p^*+r^*)-\frac{2p^*-r^*}{3}\right]$$
$$-\frac{\partial^2}{\partial\alpha\partial y}g\left[y(p^*+r^*)+\frac{p^*+r^*}{3}\right]$$
$$-\frac{\partial^2}{\partial\alpha\partial p}g\left[p(p^*+r^*)+\left(x+y-\frac{1}{3}\right)\right]$$
$$-\frac{\partial^2}{\partial\alpha\partial p^*}g[p^*(p^*+r^*)-q^*]-\frac{\partial^2}{\partial\alpha\partial q}$$
$$\times g[q(p^*+r^*)-r]-\frac{\partial^2}{\partial\alpha\partial q^*}g[q^*(p^*+r^*)]$$
$$-\frac{\partial^2}{\partial\alpha\partial r}g\left[r(p^*+r^*)-\left(y+\frac{1}{3}\right)\right]-\frac{\partial^2}{\partial\alpha\partial r^*}$$
$$\times g[r^*(p^*+r^*)]-\frac{\partial^2}{\partial\alpha^*\partial x}g\left[x(p+r)-\frac{2p-r}{3}\right]$$
$$-\frac{\partial^2}{\partial\alpha^*\partial y}g\left[y(p+r)+\frac{p+r}{3}\right]$$
$$-\frac{\partial^2}{\partial\alpha^*\partial p}g[p(p+r)-q]\ -\frac{\partial^2}{\partial\alpha^*\partial p^*}$$
$$\times g\left[p^*(p+r)+\left(x+y-\frac{1}{3}\right)\right]$$
$$-\frac{\partial^2}{\partial\alpha^*\partial q}g[q(p+r)]\ -\frac{\partial^2}{\partial\alpha^*\partial q^*}g[q^*(p+r)-r]$$
$$-\frac{\partial^2}{\partial\alpha^*\partial r}g[r(p+r)]-\frac{\partial^2}{\partial\alpha^*\partial r^*}$$
$$\left.\times g\left[r^*(p+r)-\left(y+\frac{1}{3}\right)\right]\right\}$$

$$P\, d^2\alpha\, dx\, dy\, d^2p\, d^2q\, d^2r$$

$$= \int |\alpha\rangle\langle\alpha|\, \hat{\Lambda}\, (\mathcal{L}\, P)\, d^2\alpha\, dx\, dy\, d^2p\, d^2q\, d^2r, \qquad \text{(A6)}$$

where $\mathcal{L}$ is the operator inside the curly bracket acting on P. To satisfy this equation, it is sufficient that the integrands on both sides be equal, which results in Fokker-Planck equations (11) and (12).

[1] N. A. Gershenfeld and I. L. Chuang, Science **275**, 350 (1997).
[2] J. I. Cirac and P. Zoller, Phys. Rev. Lett. **74**, 4091 (1995); K. Molmer and A. Sorensen, *ibid.* **82**, 1835 (1999).
[3] T. Pellizzari, S. A. Gardiner, J. I. Cirac, and P. Zoller, Phys. Rev. Lett. **75**, 3788 (1995).
[4] Y. Makhlin, G. Schon, and A. Schnirman, Rev. Mod. Phys. **73**, 357 (2001).
[5] L. Quiroga and N. F. Johnson, Phys. Rev. Lett. **83**, 2270 (1999); J. H. Reina, L. Quiroga, and N. F. Johnson, Phys. Rev. A **62**, 012305 (2000).
[6] Y. X. Liu, S. K. Özdemir, M. Koashi, and N. Imoto, Phys. Rev. A **65**, 042326 (2002); Y. X. Liu, A. Miranowicz, M. Koashi, and N. Imoto, *ibid.* **66**, 062309 (2002).
[7] X. Wang, M. Feng, and B. C. Sanders, Phys. Rev. A **67**, 022302 (2003).
[8] A. Imamoglu, D. D. Awschalom, G. Burkard, D. P. DiVincenzo, D. Loss, M. Sherwin, and A. Small, Phys. Rev. Lett. **83**, 4204 (1999); G. Burkard, D. Loss, and D. P. DiVincenzo, Phys. Rev. B **59**, 2070 (1999); X. Hu and S. Das Sarma, Phys. Rev. A **61**, 062301 (2000); A. Miranowicz, S. K. Özdemir, Y. X. Liu, M. Koashi, N. Imoto, and Y. Hirayama, *ibid.* **65**, 062321 (2002).
[9] G. Chen, N. H. Bonadeo, D. G. Steel, D. Gammon, D. S. Katzer, D. Park, and L. J. Sham, Science **289**, 1906 (2000); M. Bayer, P. Hawrylak, K. Hinzer, S. Fafard, M. Korkusinski, R. Wasilewski, O. Stern, and A. Forchel, *ibid*. **291**, 451 (2001).
[10] N. H. Bonadeo *et al.*, Science **282**, 1473 (1998).
[11] N. H. Bonadeo, G. Chen, D. Gammon, D. S. Katzer, D. Park, and D. G. Steel, Phys. Rev. Lett. **81**, 2759 (1998).
[12] X. Li *et al.*, Science **301**, 809 (2003).
[13] M. Winger, A. Badolato, K. J. Hennessy, E. L. Hu, and A. Imamoglu, Phys. Rev. Lett. **101**, 226808 (2008).
[14] B. W. Lovett, J. H. Reina, A. Nazir, and G. A. Briggs, Phys. Rev. B **68**, 205319 (2003).
[15] T. Unold, K. Mueller, C. Lienau, T. Elsaesser, and A. D. Wieck, Phys. Rev. Lett. **94**, 137404 (2005).
[16] P. Borri, W. Langbein, S. Schneider, U. Woggon, R. L. Sellin, D. Ouyang, and D. Bimberg, Phys. Rev. Lett. **87**, 157401 (2001).
[17] A. Blais, R.-S. Huang, A. Wallraff, S. M. Girvin, and R. J. Schoelkopf, Phys. Rev. A **69**, 062320 (2004).
[18] P. W. Shor, Phys. Rev. A **52**, R2493 (1995); A. M. Steane, Phys. Rev. Lett. **77**, 793 (1996).
[19] D. Braun, Phys. Rev. Lett. **89**, 277901 (2002).
[20] S. Clark, A. Peng, M. Gu, and S. Parkins, Phys. Rev. Lett. **91**, 177901 (2003).
[21] S. Mancini, Phys. Rev. A **73**, 010304(R) (2006).
[22] M. B. Plenio, S. F. Huelga, A. Beige, and P. L. Knight, Phys. Rev. A **59**, 2468 (1999).
[23] A. Mitra, R. Vyas, and D. Erenso, Phys. Rev. A **76**, 052317 (2007).
[24] P. D. Drummond and D. F. Walls, J. Phys. A **13**, 725 (1980).
[25] H. J. Carmichael, Phys. Rev. A **33**, 3262 (1986).
[26] C. M. Savage and H. J. Carmichael, IEEE J. Quantum Electron. **24**, 1495 (1988).
[27] C. Wang and R. Vyas, Phys. Rev. A **54**, 4453 (1996).
[28] X. Hu and K. Schulten, Physics Today **50**, Issue 8, 28 (1997).
[29] H. J. Carmichael, *Statistical Methods in Quantum Optics 1: Master Equations and Fokker-Planck Equations* (Springer, New York, 1999); *Statistical Methods in Quantum Optics 2: Non-classical Fields* (Springer, New York, 2007).
[30] W. H. Louisell, *Quantum Statistical Properties of Radiation* (Wiley, New York, 1973).
[31] C. W. Gardiner, *Handbook of Stochastic Methods for Physics, Chemistry, and the Natural Sciences* (Springer, New York, 1990).
[32] H. Risken, *The Fokker-Planck Equation: Methods of Solution and Applications* (Springer, New York, 1989).
[33] C. Wang and R. Vyas, Phys. Rev. A **51**, 2516 (1995).
[34] C. Wang and R. Vyas, Phys. Rev. A **55**, 823 (1997).
[35] D. Erenso and R. Vyas, Phys. Rev. A **65**, 063808 (2002).
[36] J. P. Gordon, Phys. Rev. **161**, 367 (1967).
[37] S. Hill and W. K. Wootters, Phys. Rev. Lett. **78**, 5022 (1997).
[38] C. H. Bennett, D. P. DiVincenzo, J. A. Smolin, and W. K. Wootters, Phys. Rev. A **54**, 3824 (1996).